

A GAMMA-RAY FLARE OF QUASAR CTA 26

J. R. MATTOX,¹ J. C. HALLUM,¹ A. P. MARSCHER,¹ S. G. JORSTAD,¹ E. B. WALTMAN,²
H. TERÄSRANTA,³ H. D. ALLER,⁴ AND M. F. ALLER⁴

Received 2000 April 12; accepted 2000 August 24

ABSTRACT

During the first 3 years of the *Compton Gamma Ray Observatory* mission, the blazar CTA 26 was observed 10 times by EGRET and not significantly detected. We report an observation in 1995 when CTA 26 flared to a peak γ -ray flux of $(4.9 \pm 1.5) \times 10^{-6} \text{ cm}^{-2} \text{ s}^{-1}$ ($E > 100 \text{ MeV}$), the third brightest of all EGRET blazars. Following the γ -ray flare, extensive VLBA and single-dish radio observations were obtained. We find two components of a milliarcsecond jet moving with apparent transverse velocities of $12 \pm 1 h^{-1} c$, and $5 \pm 2 h^{-1} c$ ($H_0 = 100 h \text{ km s}^{-1} \text{ Mpc}^{-1}$, $q_0 = 0.1$). The position angle of VLBI components appears to change with time. The slowest VLBI component's motion is consistent with ejection at the time of the 1995 γ -ray flare. A weak radio flare is also seen in Metsähovi millimeter radio monitoring data, peaking within weeks of the γ -ray flare.

Subject headings: gamma rays: observations — quasars: general — quasars: individual (CTA 26) — radio continuum: general — techniques: interferometric

1. INTRODUCTION

CTA 26 (PKS 0336–019) was originally detected as a radio source. The GHz radio spectrum is flat, with a 5 GHz flux density of $\sim 3 \text{ Jy}$. Visual identification of the radio source was made by Bolton & Ekers (1966) and verified by Kinman et al. (1967). It is classified as a quasar with a redshift $z = 0.852$ (Bolton & Wall 1970). We report here a highly significant γ -ray detection of CTA 26 in 1995 with the EGRET instrument on the *Compton Gamma Ray Observatory*.

This source was found to be optically violently variable (OVV) as the result of optical monitoring by Scott et al. (1976; see also Smith et al. 1993). Over the course of their program, CTA 26 maintained a relatively constant ($\sigma = 0.3 \text{ mag}$) flux level of about $m = 18$, punctuated by several 1 mag flares, until 1987–1988, when it brightened by $\sim 2 \text{ mag}$ over the course of 5 years. There has been no systematic monitoring of CTA 26 at optical wavelengths since 1993. It was too close to the Sun to observe optically at the time of the 1995 γ -ray flare. Polarization data are available at radio and optical wavelengths for this source. The average optical polarization measured in two observations is $11.8\% \pm 2.4\%$ (Moore & Stockman 1981), which leads to the classification of this source as a high-polarization quasar (HPQ).

CTA 26 has also been detected as an X-ray source by both the *Einstein Observatory* (Wilkes et al. 1994) and the *ROSAT All-Sky Survey* (Brinkmann et al. 1994). *Einstein* recorded a flux density at 1 keV of $0.052 \pm 0.022 \mu\text{Jy}$ in 1979 August and $0.12 \pm 0.025 \mu\text{Jy}$ in 1980 August. The *ROSAT All-Sky Survey* measured the flux density to be $1.77 \pm 0.523 \mu\text{Jy}$ at 1.3 keV in 1990. No spectral information was obtained.

This paper features a description of the EGRET results in § 2, VLBA results in § 3, radio flux density monitoring in § 4, and conclusions in § 5.

¹ Institute for Astrophysical Research, Boston University, 725 Commonwealth Avenue, Boston, MA 02215.

² Naval Research Laboratory, Code 7214, Washington, DC 20375.

³ Metsähovi Radio Observatory, Metsähovintie 114, FIN-02540 Kylmäla, Finland.

⁴ Astronomy Department, University of Michigan, Ann Arbor, MI 48109.

2. GAMMA-RAY OBSERVATIONS OF CTA 26

The Energetic Gamma-Ray Experiment Telescope (EGRET) aboard the *Compton Gamma Ray Observatory* is sensitive in the energy range 30 MeV–30 GeV (Thompson et al. 1993). It has detected over 50 AGNs (von Montigny et al. 1995; Thompson et al. 1995; Mattox et al. 1997a) in the blazar class. This classification includes BL Lac objects, HPQs, and OVV.

CTA 26 was not significantly detected by EGRET during the first 4 years of the mission, 1991.4–1995.3, although it was given significant exposure ($5.5 \times 10^8 \text{ cm}^2 \text{ s}$). A likelihood analysis (Mattox et al. 1996) of this exposure yields a 95% confidence upper limit for the average flux of $8.3 \times 10^{-8} \text{ photons cm}^{-2} \text{ s}^{-1}$, $E > 100 \text{ MeV}$.

During an exposure in the fifth year of the mission (viewing period 419.1, 1995 April 4–11), a bright γ -ray flare occurred. The EGRET instrument was pointed at the Orion cloud, 28° away from CTA 26, so the sensitivity was only $\sim 20\%$ of the on-axis sensitivity during this flare. A likelihood test (Mattox et al. 1996) gives $T_s^{1/2} = 8 \sigma$ detection significance. The average flux during this interval was $(1.8 \pm 0.4) \times 10^{-6} \text{ cm}^{-2} \text{ s}^{-1}$ ($E > 100 \text{ MeV}$). A Kolmogorov-Smirnov (KS) test (as described by Mattox et al. 1997b) finds with 99.4% confidence that the flux varied within this week. Figure 1 shows the time dependence of the flux as determined by a likelihood analysis for 1 day intervals. The flare appears to have commenced abruptly on the second day. Unfortunately, the weak exposure does not allow the rise time to be precisely determined. We can only say that a KS test indicates with 90% confidence that the onset occurred in an interval shorter than 1.3 days. The peak flux was $(4.9 \pm 1.5) \times 10^{-6} \text{ cm}^{-2} \text{ s}^{-1}$ ($E > 100 \text{ MeV}$) on 1995 April 6 (1995.263). At this time, it was the third brightest of all EGRET blazars (following PKS 1622–297 [Mattox et al. 1997b], and 3C 279 [Wehrle et al. 1998]). The γ -ray luminosity corresponding to the peak flux of CTA 26 was $1.2 \times 10^{46} (0.65/h)^2 \text{ ergs s}^{-1}$ (assuming $q_0 = 0.1$).

A likelihood position analysis (Mattox et al. 1996) of the $E > 100 \text{ MeV}$ EGRET data for the 1 week exposure during the flare gives a 95% confidence location contour which is well fit by an ellipse centered on $l = 188:25$, $b = -42:34$,

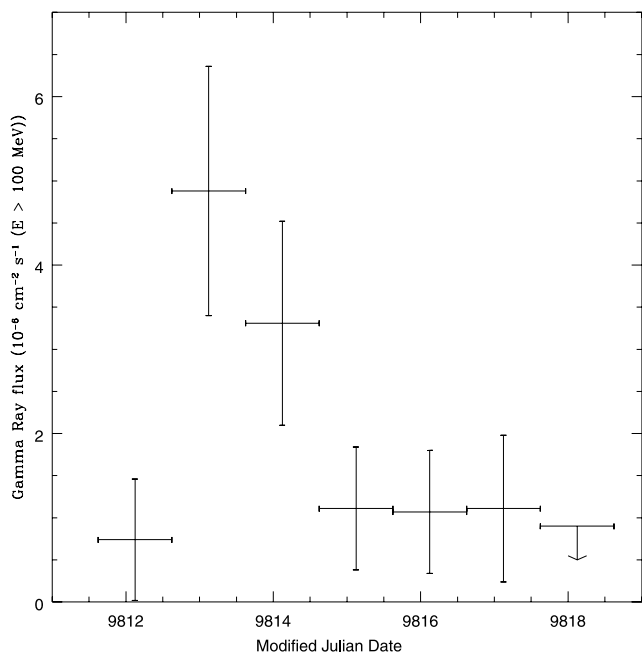


FIG. 1.—EGRET light curve for CTA 26 during the 1995 April flare. The abscissa is JD $-2,440,000.5$. The horizontal error bars indicate the interval of temporal integration. The vertical error bars indicate the range of 1σ uncertainty. The last measurement is an 84% confidence upper limit.

with semimajor axis $a = 44'$, semiminor axis $b = 37'$, and position angle $\phi = 27^\circ$. The radio position is $13'$ from the center of the ellipse. We use the method of Mattox et al. (1997a) to assess the reliability of the identification of CTA 26 as the γ -ray source. This method considers the angle between the EGRET position estimate and the radio position, the uncertainty of the EGRET position, the number density of potentially confusing radio sources as bright and with a radio spectrum as flat as CTA 26 ($8 \times 10^{-4} \text{ deg}^{-2}$), and the fraction of sources with a flat radio spectrum as bright as CTA 26 that EGRET detects (12%). The resulting probability that CTA 26 is the γ -ray source is 99.7%. The dramatic variability of the γ -ray flux lends substantial additional confidence to this identification, since the γ -ray flux from a number of other blazars has also been observed to vary wildly.

CTA 26 was also in the EGRET field of view a month later (viewing period 420, 1995 May 9–June 6). We find a detection at a lower flux level ($T_s^{1/2} = 4.3\sigma$, flux of $(0.5 \pm 0.1) \times 10^{-6} \text{ cm}^{-2} \text{ s}^{-1}$ for $E > 100 \text{ MeV}$). There is no indication of variability within viewing period 420.

2.1. The γ -Ray Spectrum of CTA 26

The γ -ray spectrum of CTA 26 was determined by performing a likelihood flux analysis (Mattox et al. 1996) for the 10 standard EGRET energy ranges using the latest EGRET data for viewing period 419.1. The EGRET point-spread function was constructed using calibration data 25° and 30° off-axis corresponding to the location of CTA 26 at 28° off-axis in viewing period 419.1. The result is shown in Figure 2. The EGRET spectrum is adequately represented by a power law:

$$F = (4.7 \pm 0.9) \times 10^{-9} \times (E/184 \text{ MeV})^{-2.4 \pm 0.3} \text{ cm}^{-2} \text{ s}^{-1} \text{ MeV}^{-1}. \quad (1)$$

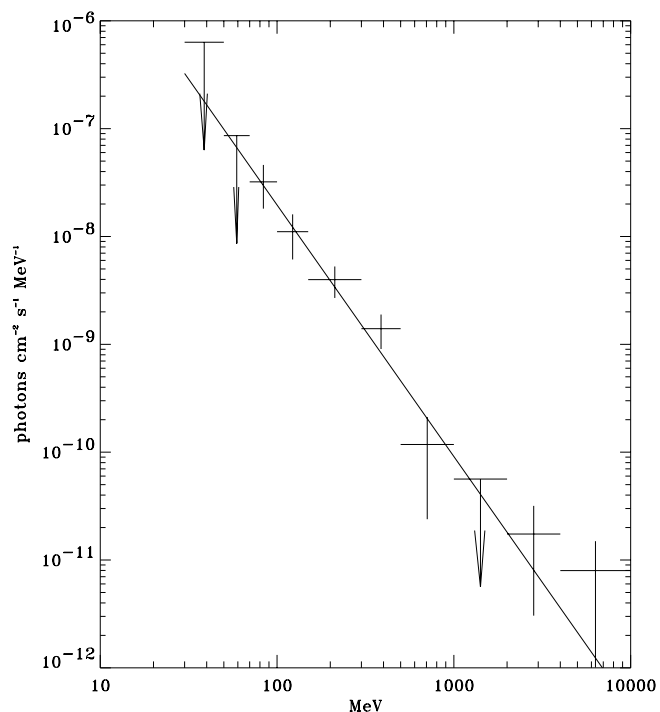


FIG. 2.—EGRET spectrum for the week of the flare in 1995 April. The straight line is the power-law representation of the spectrum given in the text.

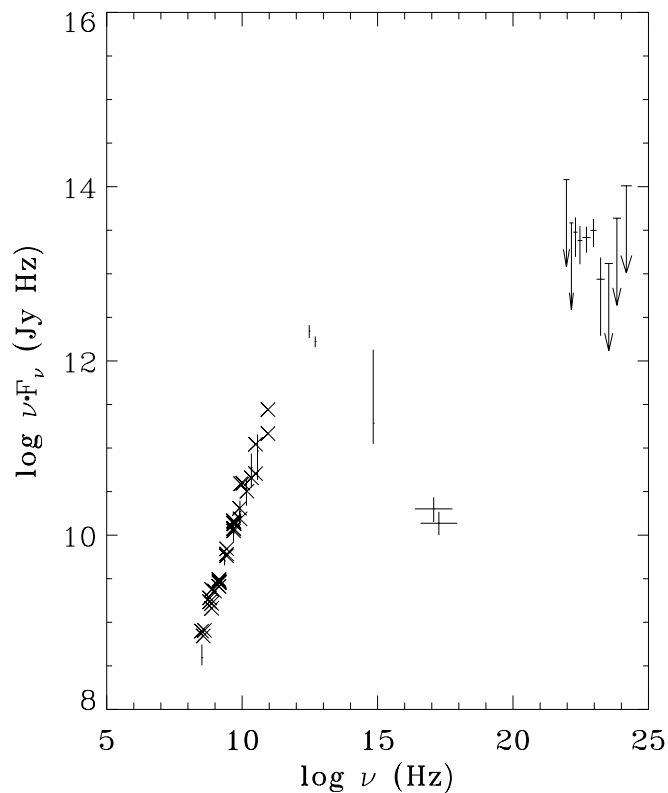


FIG. 3.—Multiwavelength spectrum of CTA 26 from observations that are not contemporaneous. The crosses indicate archival centimeter-wave radio observations from NED and the University of Michigan archive. The vertical lines in the millimeter-wave and optical regimes indicate a range of variability from multipoint observations (from NED and Scott et al. 1976, respectively). The crosses in the X-ray and γ -ray regimes show measured flux densities with uncertainties (Wilkes et al. 1994; Brinkmann et al. 1994). The γ -ray data are from EGRET. The arrows signify 95% confidence upper limits.

Figure 3 is a plot of the multiwavelength spectrum of CTA 26. The data in this plot are not contemporaneous. The synchrotron peak appears to lie somewhere in the 10^{11} – 10^{13} Hz region, and the inverse Compton peak appears to be in the GeV region. The determination of the location of the synchrotron peak is difficult, since there are no data for this source in the infrared region of the spectrum, and also because the optical flux varies by more than 1 order of magnitude over the 10 years of monitoring. The apparent γ -ray luminosity of this source during the flare is about 10 times that of the synchrotron peak, assuming that the latter did not change substantially during the γ -ray flare.

3. INTERFEROMETRIC RADIO OBSERVATIONS OF CTA 26

There have been several previous interferometric observations of CTA 26. Price et al. (1993) used the VLA to obtain an image at 20 cm (epoch 1985.0). They found a single component approximately $1''$ away from the core at a position angle of -15° . Wehrle et al. (1992) presented a VLBI map at 5 GHz, (epoch 1987.5) which showed a well-defined jet approximately 5 mas long at a position angle of 65° , nearly orthogonal to the arcsecond-scale jet. Piner & Kingham (1998) used multiple epochs of geodetic VLBI measurements from 1993–1996 at 2 and 8 GHz to measure superluminal motion of components of the milliarcsecond jet of CTA 26.

We observed CTA 26 with the Very Long Baseline Array (VLBA)⁵ in seven sessions and at three frequencies (15 GHz, 22 GHz, 43 GHz) from 1995 April to 1997 July. All observations were performed with all 10 VLBA antennas and recorded in four 8 MHz wide channels. In the first two sessions, observations were carried out during 12 hour blocks with 9–10 scans of 15–18 minutes length each at all frequencies. In the later epochs, observations were carried out as a part of a γ -ray bright blazar monitoring program (Jorstad et al. 2001) with 4–6 scans of 6–14 minutes length each. As a result, the total integration times were less at epochs following 1995 June, but there is no significant difference in resolution or dynamic range (see Table 1).

The data were correlated using the VLBA correlator in Socorro, New Mexico. Initial editing, corrections for zenith opacities and system temperatures, amplitude calibration,

⁵ The VLBA is an instrument of the National Radio Astronomy Observatory, which is operated by Associated Universities, Inc., under cooperative agreement with the National Science Foundation.

and fringe fitting were done using the standard NRAO AIPS package. Imaging was performed with the CalTech DIFMAP package (Shepherd 1997) using the procedures CLEAN and self-calibration. Uniform weighting was applied. The Metsähovi fluxes at 22 and 37 GHz and UMRAO data at 14.5 GHz were used to establish the absolute flux density scale. The observational parameters are presented in Table 1, where column (1) is the epoch of observation; (2) is the frequency; (3) is the peak flux density per beam; (4), (5), and (6) are the major axis (FWHM), minor axis, and orientation of the elliptical interferometer beam; (7) is the root mean square of the residuals of the final hybrid image; and (8) is the calibration coefficient required to match the single-dish flux densities of CTA 26 and other compact sources.

We used the task MODELFIT in DIFMAP to model the image as a number of circular Gaussian components. We determined the errors of the parameters of the components with the interactive model-fitting program SLIME in the AIPS environment. This program gives 1σ errors for the parameter values under the assumption that the data errors have a Gaussian distribution and that the parameters are independent of each other. We note that this method cannot be used for weak components (fainter than $\sim 10\%$ of the peak flux density). The results of the model fitting are given in Table 2. The first column is the epoch of observation; the second is the frequency; the third column gives the designation of the component; columns (4)–(7) give the total flux density, distance, and position angle relative to the core, and the size of the component. At all frequencies, the core is designated by the letter *A*. In what follows, we measure all motions relative to the core, which we assume to be stationary.

3.1. VLBA Results for CTA 26

The VLBA images (Figs. 4, 5, and 6) show that the source consists of a bright compact core, and a jet extending eastward to ~ 2.5 mas. The simultaneous observations at 43, 22, and 15 GHz in 1995.29 and 1995.42 allow us to estimate the spectral energy distribution of the presumed stationary core. We find that the core has an inverted spectrum (spectral index $\alpha = 0.6 \pm 0.1$, where $S \propto \nu^\alpha$). Model fitting reveals proper motions for components C3 and C4. Because of the similarity of the parameters of these components at the different frequencies, we are able to estimate their spectral indices. The spectral index of component C4 from the

TABLE 1
PARAMETERS OF VLBA OBSERVATIONS

| Epoch (1) | Frequency (GHz) (2) | S_{peak} (Jy beam ⁻¹) (3) | Θ_{maj} (mas) (4) | Θ_{min} (mas) (5) | P.A. (deg) (6) | rms (mJy beam ⁻¹) (7) | Calibration Coefficient (8) |
|--------------|---------------------------|--|---------------------------------------|---------------------------------------|----------------------|---|-----------------------------------|
| 1995.29..... | 15.4 | 0.86 | 0.97 | 0.40 | -4 | 1.49 | 1.37 ± 0.10 |
| 1995.42..... | 15.4 | 1.17 | 0.98 | 0.38 | -6 | 0.75 | 1.06 ± 0.10 |
| 1995.29..... | 22.2 | 1.33 | 0.73 | 0.30 | -8 | 1.22 | 1.18 ± 0.10 |
| 1995.42..... | 22.2 | 1.16 | 0.74 | 0.28 | -9 | 0.98 | 1.00 ± 0.10 |
| 1996.34..... | 22.2 | 0.86 | 0.75 | 0.30 | -7 | 0.72 | 1.18 ± 0.10 |
| 1996.60..... | 22.2 | 1.10 | 0.76 | 0.31 | -10 | 1.15 | 1.02 ± 0.10 |
| 1996.90..... | 22.2 | 1.61 | 0.78 | 0.30 | -8 | 1.24 | 1.39 ± 0.10 |
| 1995.29..... | 43.2 | 1.53 | 0.36 | 0.15 | -6 | 1.52 | 1.30 ± 0.20 |
| 1995.42..... | 43.2 | 1.92 | 0.37 | 0.15 | -7 | 1.85 | 1.57 ± 0.20 |
| 1995.58..... | 43.2 | 2.18 | 0.39 | 0.15 | -10 | 4.45 | 1.60 ± 0.20 |
| 1996.90..... | 43.2 | 1.68 | 0.38 | 0.15 | -2 | 2.23 | 1.40 ± 0.20 |
| 1997.58..... | 43.2 | 1.66 | 0.42 | 0.19 | +7 | 2.67 | 1.23 ± 0.20 |

TABLE 2
MODEL PARAMETERS

| Epoch (1) | Frequency (GHz) (2) | Component (3) | Flux (Jy) (4) | R (mas) (5) | Θ (deg) (6) | a (mas) (7) |
|--------------|---------------------------|------------------|---------------------|-------------------|--------------------------|---------------------|
| 1995.29..... | 15.4 | A | 0.81 ± 0.06 | 0.0 ± 0.05 | | 0.12 ± 0.05 |
| | | C3 | 0.44 ± 0.07 | 0.33 ± 0.08 | $+67 \pm 5$ | 0.25 ± 0.06 |
| | | C2 | 0.37 ± 0.06 | 0.89 ± 0.10 | $+72 \pm 4$ | 0.88 ± 0.07 |
| | | C1 | 0.04 | 2.03 | +68 | 0.31 |
| 1995.42..... | 15.4 | A | 1.26 ± 0.04 | 0.0 ± 0.06 | | 0.09 ± 0.04 |
| | | C3 | 0.31 ± 0.05 | 0.54 ± 0.07 | $+55 \pm 6$ | 0.41 ± 0.05 |
| | | C2 | 0.33 ± 0.04 | 1.05 ± 0.10 | $+69 \pm 5$ | 0.82 ± 0.06 |
| | | C1 | 0.05 | 2.05 | +65 | 0.43 |
| 1995.29..... | 22.2 | A | 1.46 ± 0.04 | 0.0 ± 0.04 | | 0.13 ± 0.05 |
| | | C3 | 0.38 ± 0.05 | 0.48 ± 0.06 | $+57 \pm 4$ | 0.53 ± 0.05 |
| | | C2 | 0.25 ± 0.07 | 1.06 ± 0.12 | $+72 \pm 5$ | 0.87 ± 0.09 |
| | | C1 | 0.02 | 2.46 | +60 | 0.52 |
| 1995.42..... | 22.2 | A | 1.20 ± 0.05 | 0.0 ± 0.05 | | 0.02 ± 0.02 |
| | | C3 | 0.26 ± 0.04 | 0.65 ± 0.08 | $+54 \pm 3$ | 0.48 ± 0.06 |
| | | C2 | 0.15 ± 0.05 | 1.24 ± 0.10 | $+73 \pm 5$ | 0.88 ± 0.07 |
| | | C1 | 0.01 | 2.21 | +59 | 0.32 |
| 1996.34..... | 22.2 | A | 0.67 ± 0.06 | 0.0 ± 0.05 | | 0.03 ± 0.02 |
| | | C4 | 0.38 ± 0.04 | 0.20 ± 0.06 | $+29 \pm 4$ | 0.24 ± 0.06 |
| | | C2 | 0.02 | 1.24 | +94 | 0.01 |
| | | C3 | 0.33 ± 0.05 | 1.08 ± 0.06 | $+65 \pm 5$ | 0.83 ± 0.05 |
| | | C1 | 0.05 | 2.33 | +56 | 1.50 |
| 1996.60..... | 22.2 | A | 1.13 ± 0.04 | 0.0 ± 0.04 | | 0.05 ± 0.03 |
| | | C4 | 0.12 ± 0.05 | 0.28 ± 0.07 | $+49 \pm 5$ | 0.01 ± 0.03 |
| | | C3 | 0.36 ± 0.05 | 1.24 ± 0.08 | $+66 \pm 4$ | 0.94 ± 0.06 |
| | | C1 | 0.02 | 2.67 | +56 | 0.56 |
| 1996.90..... | 22.2 | A | 1.65 ± 0.04 | 0.0 ± 0.04 | | 0.00 ± 0.03 |
| | | C4 | 0.11 ± 0.05 | 0.30 ± 0.09 | $+53 \pm 4$ | 0.05 ± 0.03 |
| | | C3 | 0.21 ± 0.05 | 1.23 ± 0.10 | $+73 \pm 4$ | 0.57 ± 0.05 |
| | | C1 | 0.06 | 2.78 | +57 | 1.30 |
| 1995.29..... | 43.2 | A | 1.74 ± 0.05 | 0.0 ± 0.03 | | 0.08 ± 0.03 |
| | | C3 | 0.22 ± 0.04 | 0.47 ± 0.09 | $+51 \pm 3$ | 0.42 ± 0.04 |
| | | C2 | 0.17 ± 0.05 | 1.02 ± 0.08 | $+70 \pm 4$ | 0.78 ± 0.07 |
| 1995.42..... | 43.2 | A | 1.96 ± 0.07 | 0.0 ± 0.04 | | 0.03 ± 0.03 |
| | | B | 0.06 | 0.45 | +42 | 0.01 |
| | | C3 | 0.27 ± 0.05 | 0.74 ± 0.06 | $+61 \pm 3$ | 0.61 ± 0.04 |
| | | C2 | 0.05 | 1.38 | +83 | 0.29 |
| 1995.58..... | 43.2 | A | 2.19 ± 0.05 | 0.0 ± 0.04 | | 0.04 ± 0.03 |
| | | C4 | 0.33 ± 0.07 | 0.17 ± 0.06 | $+23 \pm 7$ | 0.13 ± 0.05 |
| | | C3 | 0.29 ± 0.05 | 0.75 ± 0.08 | $+54 \pm 4$ | 0.44 ± 0.05 |
| | | C2 | 0.09 | 1.31 | +79 | 0.48 |
| 1996.90..... | 43.2 | A | 1.69 ± 0.04 | 0.0 ± 0.04 | | 0.03 ± 0.03 |
| | | C4 | 0.09 ± 0.05 | 0.27 ± 0.05 | $+49 \pm 6$ | 0.17 ± 0.04 |
| | | C3 | 0.19 ± 0.04 | 1.29 ± 0.07 | $+66 \pm 4$ | 0.83 ± 0.05 |
| 1997.59..... | 43.2 | A | 1.75 ± 0.05 | 0.0 ± 0.04 | | 0.08 ± 0.04 |
| | | C5 | 0.19 ± 0.04 | 0.19 ± 0.06 | $+37 \pm 5$ | 0.23 ± 0.05 |
| | | C4 | 0.02 | 0.43 | +53 | 0.01 |
| | | C3 | 0.15 ± 0.05 | 1.45 ± 0.10 | $+70 \pm 4$ | 0.98 ± 0.07 |

22 and 43 GHz observations is $\alpha = -0.31 \pm 0.09$ at epoch 1996.90. The spectral index of component C3 at 15–43 GHz changes from a typical spectrum of an optically thin synchrotron source ($\alpha = -0.68 \pm 0.14$) at epoch 1995.29 to a flatter spectrum at epoch 1995.42 ($\alpha = -0.11 \pm 0.26$). The change in spectrum reflects an increase of the flux at 43 GHz while it fades at 22 and 15 GHz. We note that component C3 reaches the observed maximum flux at 43 GHz at epoch 1995.58 at a distance of 0.75 mas from the core.

Figure 7 shows the time dependence of the relative separation between the core and components. For components C3 and C4, a linear fit to the data yields an appar-

ent angular separation rate of $\mu_3 = 0.42 \pm 0.04$ and $\mu_4 = 0.18 \pm 0.07$ mas yr⁻¹, respectively. The corresponding transverse velocities are $12 \pm 1 h^{-1} c$, and $5 \pm 2 h^{-1} c$ for $H_0 = 100 h$ km s⁻¹ Mpc⁻¹, and $q_0 = 0.1$. Linear back-extrapolation of the motion of component C3 gives the epoch of zero separation as 1993.9 ± 0.1 , which corresponds within an uncertainty of 2σ to the epoch of zero separation of 1993.3 ± 0.3 reported by Piner & Kingham (1998) for their component C3. They found a velocity of $7.1 \pm 0.9 h^{-1} c$ (converting their value to $q_0 = 0.1$) for this component, which is less than the velocity we measure.

Our component C4 was not detected by Piner & Kingham (1998), who reported no new VLBI component

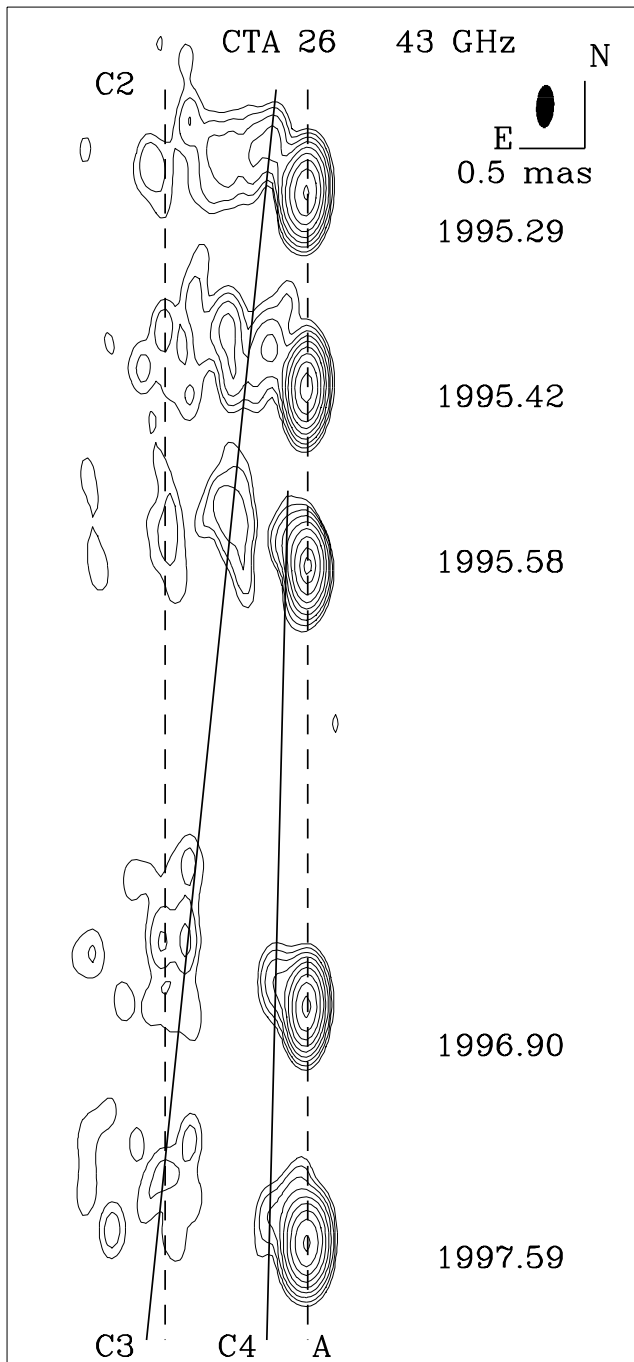


FIG. 4.—Hybrid VLBA maps at 43 GHz. The contour levels are 0.5%, 1%, 2%, 4%, 8%, 16%, 32%, 64%, and 90% of the peak intensity seen at epoch 1995.58, $2.18 \text{ Jy beam}^{-1}$. The restoring beam ($0.35 \times 0.15 \text{ mas}^2$ at P.A. = -2° , shown at the upper right) is an average of the beam (which varies little) over all epochs. The dashed lines indicate the mean positions of the core (A) and a stationary feature (C2). The solid lines indicate the least-squares fit to the proper motions of moving components C3 and C4.

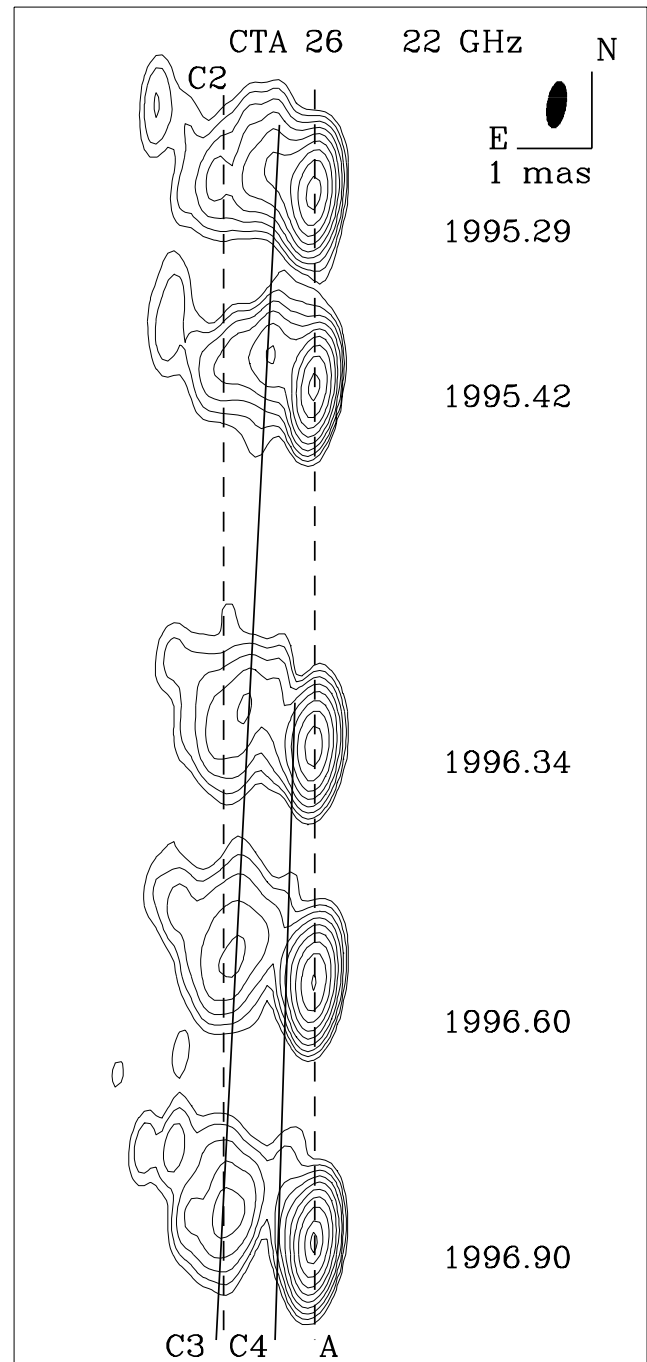


FIG. 5.—Hybrid maps at 22 GHz. The contour levels are 0.25%, 0.5%, 1%, 2%, 4%, 8%, 16%, 32%, 64%, and 90% of the peak intensity seen at epoch 1996.90, $1.60 \text{ Jy beam}^{-1}$. The restoring beam ($0.75 \times 0.30 \text{ mas}^2$ at P.A. = -8° , shown at the upper right) is an average of the beam (which varies little) over all epochs. The dashed lines indicate the mean positions of the core (A) and a stationary feature (C2). The solid lines indicate the least-squares fit to the proper motions of moving components C3 and C4.

corresponding to the CTA 26 γ -ray flare. Linear back-extrapolation of the motion of component C4 gives an epoch of zero separation of 1995.13 ± 0.16 , which is consistent with the 1995.263 epoch of the γ -ray flare reported in § 2 of this paper. This could be a chance coincidence: Piner & Kingham (1998) also report no new VLBI components corresponding to the EGRET detection of γ -ray flares from sources 1156 + 295 and 1606 + 106. On the other hand, from

a comparison of times of γ -ray flares and times of the origin of new VLBI components as measured using the VLBA for a larger number of blazars (19), Marchenko-Jorstad et al. (2000) found that a statistically significant fraction (but not all) of γ -ray flares correspond to the ejection of new superluminal VLBI components.

We also identify two additional components, C1 and C2. Component C1 is very weak and is not detected at 43 GHz;

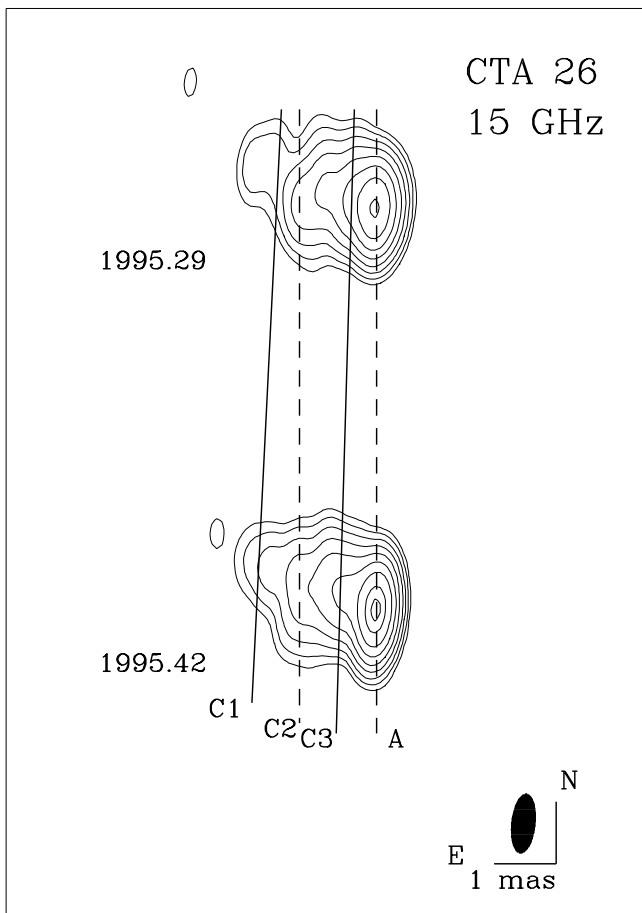


FIG. 6.—Hybrid maps at 15 GHz; contour levels are 0.5%, 1%, 2%, 4%, 8%, 16%, 32%, 64%, and 90% of the peak intensity seen at epoch 1995.42, $1.17 \text{ Jy beam}^{-1}$. The restoring beam ($0.98 \times 0.40 \text{ mas}^2$ at P.A. = -4° , shown at the bottom right) is an average of the beam (which varies little) between epochs. The dashed lines indicate the mean positions of the core (A) and a stationary feature (C2). The solid lines indicate the least-squares fit to the proper motions of moving components C1 and C3.

at 22 GHz a superluminal velocity of $7 \pm 4 h^{-1} c$ is found. Component C2 is detected at all frequencies during 1995 and is found to have a steep spectrum with $\alpha = -0.73 \pm 0.09$. We conclude that it is most likely a stationary feature at a position where the jet bends. It is blended with component C3 in the 1996 images as the latter passes by.

In Figure 8 the measured position angles are shown as a function of distance from the core. Our data indicate that the direction of the jet changes substantially with distance from the core, as first suggested by Piner & Kingham (1998) based on lower resolution images. We observe components emerging along a position angle of $\sim 20^\circ$ near the core. The position angle then appears to increase gradually, reaching $\sim 80^\circ$ at 1.2 mas, where stationary feature C2 is located, but then apparently decreases to $\sim 55^\circ$ beyond $\sim 2 \text{ mas}$.

Moving components C1, C3, and C4 are observed at different locations in a bending jet at significantly different apparent velocities. This may be explained if the jet is helical, as proposed to explain a number of blazars with curved jets and variable apparent motion (e.g., 3C 345: Hardee 1987; Mrk 501: Conway & Wrobel 1995). If we assume that each component of the CTA 26 jet has the same Lorentz factor ($\Gamma_{\text{min}} = 18.5$, the minimum required to

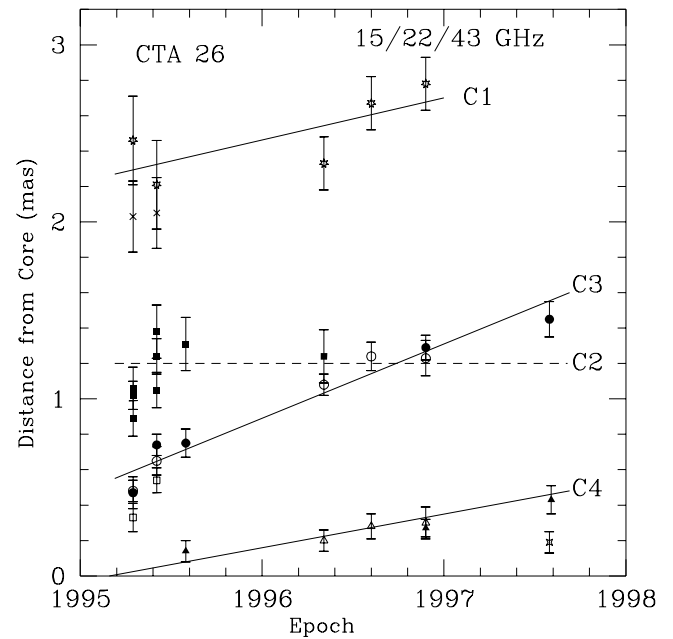


FIG. 7.—VLBA measurements of the time dependence of the separation of CTA 26 jet components from the core. For component C1, the open stars represent the distance for the 22 GHz model, and the crosses indicate the distance for the 15 GHz model. For component C2, filled squares are used at all frequencies. For component C3, filled circles represent positions obtained from the 43 GHz model, open circles the 22 GHz model, and open squares the 15 GHz model. For component C4, filled triangles represent positions obtained from the 43 GHz model, and open triangles the 22 GHz model. Component C5, which is detected only during the last observation at 43 GHz, is shown with a four-sided square. The linear fit of proper motion for components C3 and C4 is calculated using the data at 43 and 22 GHz; in the case of component C1 only the data at 22 GHz are used.

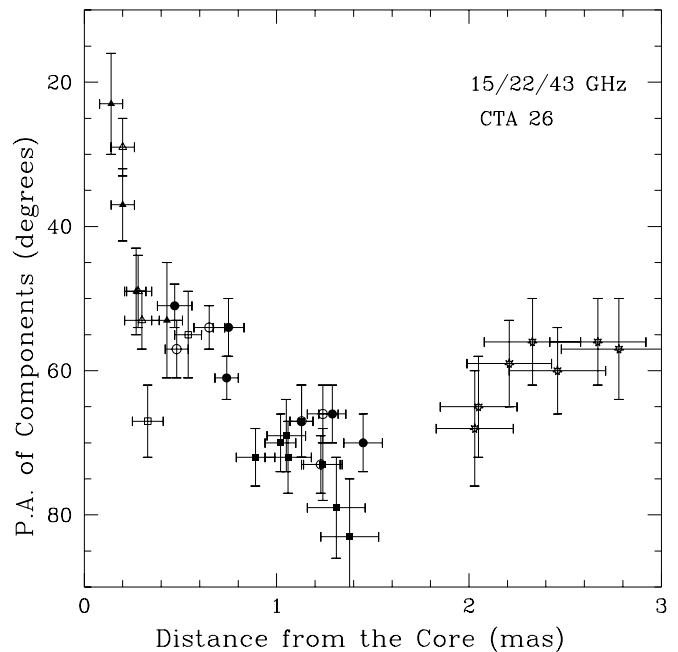


FIG. 8.—Measured position angles (measured from north through east) and distance from the core for all CTA 26 components at all frequencies and all epochs. Component C1 is shown with open stars at all frequencies; component C2 is shown with filled squares at all frequencies; component C3 is shown with filled circles at 43 GHz, with open circles at 22 GHz, and with open squares at 15 GHz; component C4 is shown with filled triangles at 43 GHz and open triangles at 22 GHz.

explain the apparent velocity of $12 h^{-1} c$ observed for component C3 at the optimal viewing angle, $\theta = \arcsin \Gamma^{-1} = 3^\circ.1$, assuming $h = 0.65$), then the lower apparent velocities of components C4 and C1 may be caused by suboptimal viewing angles due to helical motion of the jet. The $5 h^{-1} c$ velocity of component C4 near the core could result from a viewing angle of either $0^\circ.7$ or $14^\circ.1$, while the $7 h^{-1} c$ velocity of component C1 > 2 mas from the core corresponds to a viewing angle of either $1^\circ.0$ or $9^\circ.6$. The larger angles imply bends which are expected to be too severe given the high momentum expected for a relativistic jet.

4. RADIO FLUX DENSITY MONITORING OF CTA 26

There have been several investigations of the possible correlation between the γ -ray flux and the radio flux of blazars. Mattox et al. (1997a) noted that all bright γ -ray blazars also emit substantial radio flux, which implies with a statistical confidence of 0.9998 that there is some correlation between the radio and γ -ray properties of blazars. Reich et al. (1993) suggest that high γ -ray states seem to be related with high centimeter radio states but that the radio is sometimes delayed by a few months. However, Mücke et

al. (1997) find no linear correlation between either simultaneous or average measurements of centimeter flux and γ -ray flux.

A possible explanation for the lack of correlation reported by Mücke et al. (1997) is that centimeter radiation is self-absorbed in the region of the jet where γ -rays originate, and comes predominantly from farther out. Valtaoja & Teräsanta (1995) claim that γ -ray flares occur near the start of a general rise or near maximum millimeter wavelength flux. Bower et al. (1997) found in the case of NRAO 530 that an increase in millimeter flux was correlated with a rise in the γ -ray flux detected by EGRET, but that γ -ray detections did not always occur during or immediately prior to a millimeter wavelength flare.

The radio flux density of CTA 26 was monitored extensively with single-dish radio telescopes at diverse frequencies by a number of groups. Figure 9 displays radio light curves spanning 2 decades at seven radio frequencies. This flux density has been quite variable, with peaks at 8.0 GHz in 1982, 1987, 1990, and 1993.

During the era of the 1995 γ -ray flare, CTA 26 was being monitored at 22 GHz and 37 GHz at the Metsähovi Radio

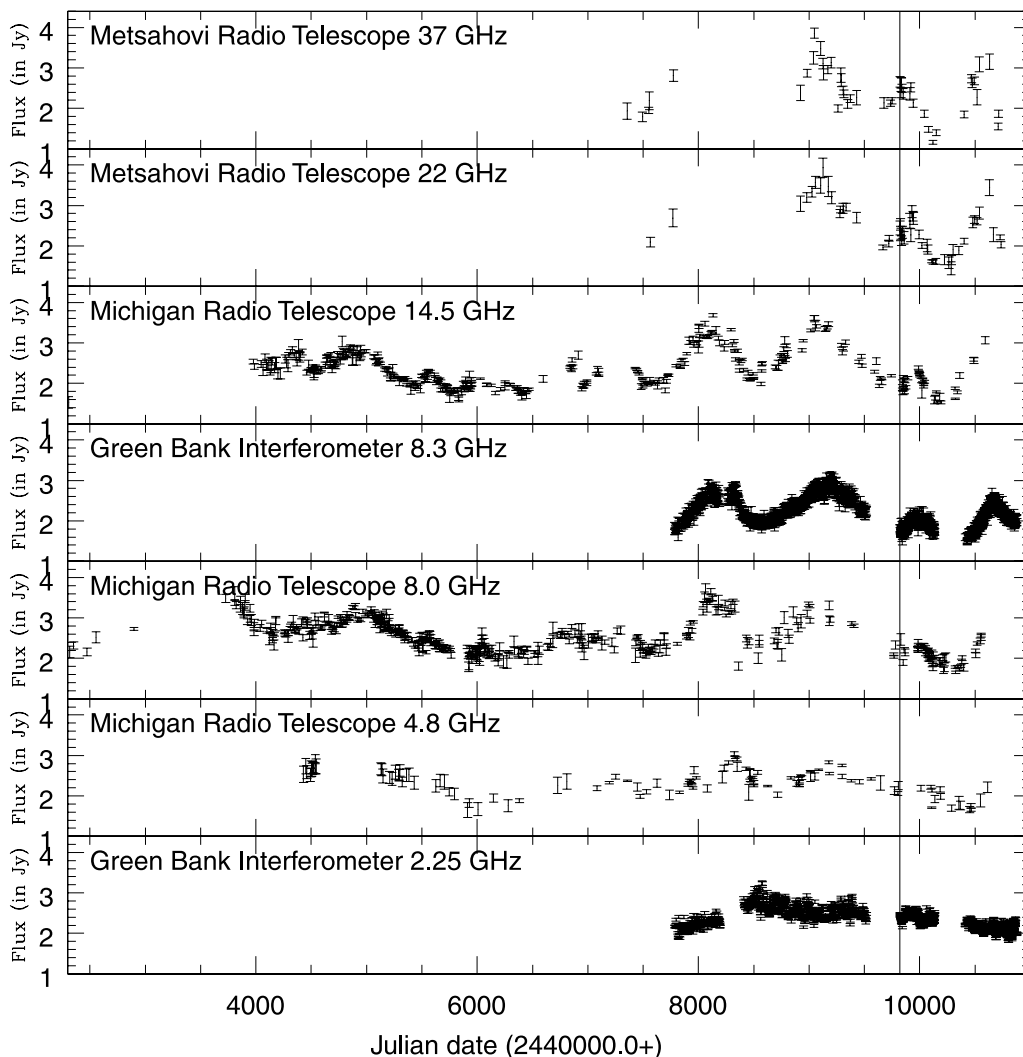


FIG. 9.—Light curves at the seven most frequently monitored radio frequencies between 1974 and 1998. The vertical line at MJD 9811 signifies the epoch of the γ -ray flare reported in § 2.

Research station, and at 4.8, 8.0, and 14.8 GHz with the University of Michigan Radio Observatory. Monitoring at 2.25 and 8.3 GHz with the Green Bank Interferometer occurred until 1994 May, and then resumed when the GBI group was informed of the γ -ray flare reported in § 2. The radio light curves during the era of the γ -ray flare are shown in Figure 10. A modest radio flare is observed to follow the γ -ray flare. Because these observations include flux from all radio components, it is not possible to extract detailed information on the radio flare. However, the data are consistent with a radio flare which peaks at 37 GHz within weeks of the time of the γ -ray flare, and is also apparent later at lower frequencies at a reduced amplitude as expected for an expanding plasma. Because this radio flare is weak (larger flares are apparent in 1994 and 1997), it cannot be uniquely associated with the γ -ray flare given the potential range of delays possible for the emergence of a radio flare following a γ -ray flare. However, the contemporaneous emergence of a superluminal VLBI component adds weight to the possibility of an association.

We note a possible correspondence between the radio flare of 1993, which peaks at 37 GHz at 1993.38, and the extrapolated ejection of component C3 at 1993.9 ± 0.1 . Also, there is a possible correspondence between the radio flare of 1997, which peaks at 37 GHz at 1997.25, and the

ejection of component C5, which is first seen at 1997.59. There were no EGRET observations of CTA 26 during the 1993 and 1997 radio flares.

5. CONCLUSIONS

We report a dramatic γ -ray flare for blazar CTA 26, showing at peak the third largest γ -ray flux of any of the blazars observed by EGRET. The γ -ray flux increase was rapid, at least a factor of 4 in less than 1.3 days. A weak radio flare was observed to peak within weeks of the γ -ray flare. Post-flare VLBI results are presented. In these images we detect several radio components. One component existed at the time of the flare and is observed to have an apparent transverse velocity of $12 \pm 1 h^{-1} c$. A second component is visible in images starting in 1996 and shows an apparent transverse velocity of $5 \pm 2 h^{-1} c$. A linear extrapolation of the motion of the slower component indicates an origin at the core at a time consistent with the γ -ray flare. An additional possible component is seen with a superluminal velocity of $7 \pm 4 h^{-1} c$.

J. R. M. acknowledges support from NASA grant NAG5-3384. The work of A. P. M. and S. G. J. was supported in part by NASA grants NAG 5-7323 and NAG 5-2508, and National Science Foundation grant AST 98-02941. This

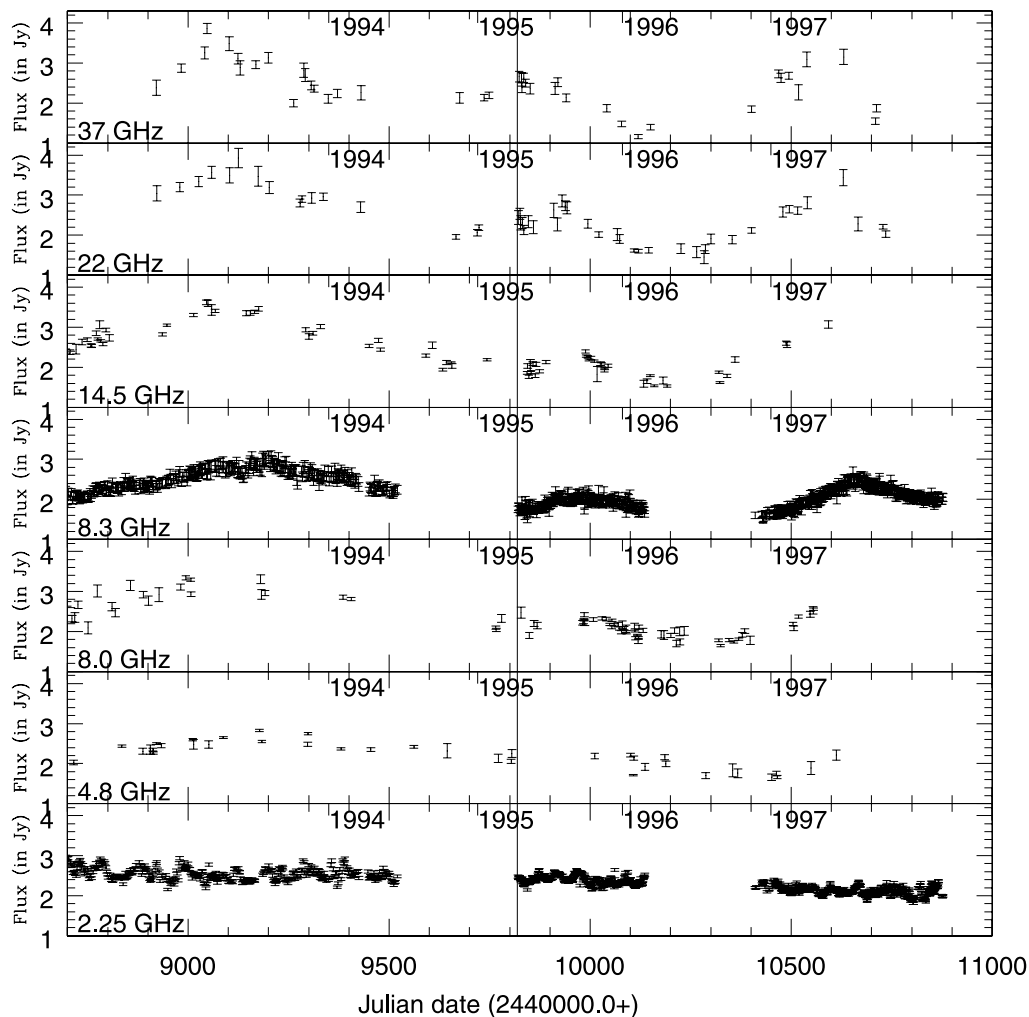


FIG. 10.—Light curves for seven radio frequencies between 1993 and 1998. The vertical line marks 1995.263, the epoch of the γ -ray flare reported in § 2.

research has made use of data from the University of Michigan Radio Astronomy Observatory, which is supported by the National Science Foundation, and by funds from the University of Michigan. The Green Bank Interferometer is a facility of the National Science Foundation operated by the National Radio Astronomy Observatory with partial support for the monitoring program provided by the U.S. Naval Observatory and the NASA High Energy programs. Radio astronomy at the Naval Research Laboratory is

supported by the Office of Naval Research. This research has made use of the NASA/IPAC Extragalactic Database (NED), which is operated by the Jet Propulsion Laboratory, California Institute of Technology, under contract with the National Aeronautics and Space Administration. We also wish to express gratitude for the opportunity to use the EGRET analysis facilities of the Compton Observatory Science Support Center in support of this work.

REFERENCES

- Bolton, J. G., & Ekers, J. 1966, *Australian J. Phys.*, 19, 559
 Bolton, J. G., & Wall, J. V. 1970, *Australian J. Phys.*, 23, 789
 Bower, G. C., et al. 1997, *AJ*, 484, 118
 Brinkmann, W., Siebert, J., & Boller, T. 1994, *A&A*, 281, 355
 Conway, J. E., & Wrobel, J. M. 1995, *ApJ*, 439, 98
 Hardee, P. E. 1987, *ApJ*, 318, 78
 Jorstad, S. G., Marscher, A. P., Wehrle, A. E., Mattox, J. R., & Bloom, S. D. 2001, *ApJS*, in press
 Kinman, T. J., et al. 1967, *ApJ*, 147, 848
 Marchenko-Jorstad, S. G., et al. 2000, in *Astrophysical Phenomena Revealed by Space VLBI*, ed. H. Hirabayashi, P. G. Edwards, & D. W. Murphy (Japan: Inst. of Space and Astronautical Science), 305
 Mattox, J. R., et al. 1996, *ApJ*, 461, 396
 Mattox, J. R., Schachter, J., Hartman, R. C., Molnar, L., & Patnaik, A. R. 1997a, *ApJ*, 481, 95
 Mattox, J. R., Wagner, S., Malkan, M., McGlynn, T. A., Schachter, J. F., Grove, J. E., Johnson, W. N., & Kurfess, J. D. 1997b, *ApJ*, 476, 692
 Moore, R. L., & Stockman, H. S. 1981, *ApJ*, 243, 60
 Mücke, A., et al. 1997, *A&A*, 320, 33
 Owen, F. N., Procas, R. W., & Neff, S. G. 1978, *AJ*, 83, 1009
 Owen F. N., Spangler, S. R., & Cotton, W. D. 1980, *AJ*, 85, 351
 Pauliny-Toth, I. I. K., et al. 1972, *AJ*, 83, 451
 Piner, B. G., & Kingham, K. A. 1998, *ApJ*, 507, 706
 Price, R., Gower, A. C., Hutchings, J. B., Talon, S., Duncan, D., & Ross, G. 1993, *ApJS*, 86, 365
 Reich, W., et al. 1993, *A&A*, 273, 65
 Reuter, H. P., et al. 1997, *A&AS*, 122, 271
 Scott, R. L., et al. 1976, *AJ*, 81, 7
 Shepherd, M. C., 1997, in *ASP Conf. Ser. 125, Astronomical Data Analysis Software and Systems*, ed. G. Hunt & H. E. Payne (San Francisco: ASP), 77
 Smith A. D., et al. 1993, *AJ*, 105, 437
 Thompson, D. J., et al. 1993, *ApJS*, 86, 629
 ———. 1995, *ApJS*, 101, 259
 Valtaoja, E., & Teräsanta, H. 1995, *A&A*, 297, 13
 von Montigny, C., et al. 1995, *ApJ*, 440, 525
 Waltman, E., et al. 1991, *ApJS*, 77, 379
 Wehrle, A. E., et al. 1992, *ApJ*, 391, 589
 ———. 1998, *ApJ*, 497, 178
 Wilkes, B. J., et al. 1994, *ApJS*, 92, 53